Advantages of Multi-shell Diffusion Models for Studies of Brain Development in Youth

Adam R. Pines[1], Matthew Cieslak[1], Graham L. Baum[1], Philip A. Cook[2], Azeez Adebimpe[1], Diego G. Dávila,[1] Mark A. Elliott[2], Robert Jirsaraie[1], Kristin Murtha[1], Desmond J. Oathes,[1] Kayla Piiwaa[1], Adon F. G. Rosen[1], Sage Rush[1], Russell T. Shinohara[3], Danielle S. Bassett,[1,4-7] David R. Roalf[1], & Theodore D. Satterthwaite[1]*

1. Department of Psychiatry, University of Pennsylvania, Philadelphia, PA 19104
2. Department of Radiology, University of Pennsylvania, Philadelphia, PA 19104
3. Department of Biostatistics, Epidemiology, and Informatics University of Pennsylvania, Philadelphia, PA 19104
4. Department of Bioengineering, University of Pennsylvania, Philadelphia, PA 19104
5. Department of Electrical and Systems Engineering, University of Pennsylvania, Philadelphia, PA 19104
6. Department of Physics and Astronomy, University of Pennsylvania, Philadelphia, PA 19104
7. Department of Neurology, University of Pennsylvania, Philadelphia, PA 19104

*Please address correspondence to:
Theodore D. Satterthwaite
Department of Psychiatry
University of Pennsylvania
Philadelphia, PA 19104

ABSTRACT

Diffusion-weighted imaging (DWI) has advanced our understanding of how brain microstructure evolves during neurodevelopment. Most existing studies of brain development use a simple scalar measure — fractional anisotropy (FA) — to characterize brain tissue microstructure. However, advances in the modeling of diffusion images, such as Neurite Orientation Dispersion and Density Imaging (NODDI) and Laplacian-regularized Mean Apparent Propagator MRI (MAPL), allow for greater richness in how microstructure is characterized. Nonetheless, the differential utility of these new diffusion models for understanding brain development remains sparsely investigated. Additionally, despite ample evidence that motion artifact is a major confound for studies of brain development, the relative vulnerability of these models to in-scanner motion has not been described. Accordingly, in a sample of 123 youth (ages 12-30) we evaluated FA in comparison to two recently introduced diffusion metrics: intra-cellular volume fraction (ICVF) from NODDI and return-to-origin probability (RTOP) from MAPL. Associations with age were evaluated for each of these measures at multiple scales, including mean white matter scalar values, voxelwise analyses, and tractography-based networks. Additionally, we examined the association between in-scanner head motion and each of these measures. Our results reveal that ICVF and RTOP are more associated with development than FA, and are less impacted by motion. Collectively, our findings suggest that multi-shell diffusion models confer notable advantages over FA for studies of the developing brain.

KEYWORDS: Diffusion-weighted imaging; Development; Multi-shell diffusion; Artifact; Confound; Structural connectivity; Motion

1. INTRODUCTION

Diffusion-weighted imaging (DWI) has informed our understanding of both local tissue (Basser and Pierpaoli 1996; Koh and Padhani 2006; Svolos et al., 2014) and distributed network properties of the brain *in vivo* (Sporns, Tononi, and Kötter 2005; Gollo et al., 2018). DWI has proven to be particularly useful for studying neurodevelopment, and has provided critical evidence of the protracted maturation of white matter from infancy into adulthood (Lebel et al., 2008; Schmithorst and Yuan 2010). Recent studies have leveraged tools from network neuroscience and established that structural networks reconfigure in development to promote efficient communication (Hagmann et al., 2010; Fan et al., 2011; Grayson et al., 2014; Baum et al., 2017; Uddin et al., 2011; Baker et al., 2015; Bassett, Zurn, & Gold, 2018; Huang et al., 2015).

Most studies which have used DWI to study brain development have used the diffusion tensor model (Lebel & Deoni, 2018; Lebel, Treit, & Beaulieu, 2017). While valuable, these studies may have been limited by certain characteristics of diffusion tensor model. Specifically, DTI-derived metrics such as fractional anisotropy (FA) systematically underestimate diffusion restriction in voxels with crossing fibers (Jeurissen et al., 2013; Jones and Cercignani 2010; Volz, Cieslak, and Grafton 2018; De Santis et al., 2014). Furthermore, FA has been shown to be impacted by in-scanner motion, which is often prominent in children (Yendiki et al., 2014; Ling et al., 2012; Baum et al., 2018; Roalf et al., 2016). More recently, a new generation of models have been developed to leverage multiple *b*-values ("shells") that can be collected during a DWI scan. These models can be broadly separated into "tissue" and "signal" models (Alexander et al., 2017; Ferizi et al., 2017): tissue models attempt to classify signal attributable to different classes of biological tissues, while signal models do not attempt to delineate tissue classes.

Although several tissue models were foundational for multi-compartment modeling of diffusion images (Assaf and Basser 2005; Alexander et al., 2010), Neurite Orientation Dispersion and Density Imaging has become the most widely used (NODDI; Zhang et al., 2012). NODDI estimates the directional distribution of neurites (axons and dendrites) in a voxel, and then matches diffusion patterns to that distribution to estimate the Intracellular Volume Fraction (ICVF) of a voxel. Recent work suggests that NODDI may be more attuned to biological features of brain development than DTI (Chang et al., 2015; Genc et al., 2017; Nazeri et al., 2015; Ota et al., 2017; Mah, Geeraert, and Lebel 2017; Eaton-Rosen et al., 2015; Deligianni et al., 2016; Ota et al., 2017). However, it remains unclear as to how useful NODDI-based measures such as ICVF are for studies of brain networks, or how ICVF is impacted by in-scanner motion.

In contrast to tissue-based models like NODDI, "signal" based methods use the Fourier relationship between *q*-space signal and the ensemble average propagator (EAP) to characterize the intra-voxel diffusion process. Two recently-introduced techniques which model the EAP are Mean Apparent Propagator MRI (MAP-MRI; Özarslan et al., 2013) and Laplacian-regularized MAP-MRI (MAPL; Fick et al., 2016). These models allow estimation of the return-to-origin probability (RTOP), which indicates the likelihood of water molecules undergoing no net displacement in a particular voxel (Özarslan et al., 2013). In contrast to the accumulating number of studies which have used NODDI to study brain development, the utility of MAPL for studying brain development in youth has not been described. Furthermore, like NODDI, it remains unknown how motion may impact EAP-based measures such as RTOP.

Accordingly, here we sought to describe the differential sensitivity of three diffusion models to both brain development and in-scanner motion. Specifically, we evaluated how FA (from DTI), ICVF (from NODDI), and RTOP (from MAPL) are associated with both age and in-scanner motion in a sample of 123 youth who completed multi-shell diffusion imaging. These associations were examined at multiple scales, including mean white matter values, voxelwise analyses, and tractography-based networks. As described below, we present new evidence that suggests that

contemporary diffusion models such as NODDI and MAPL may be both more sensitive to brain development and less confounded by in-scanner motion.

2. METHODS

2.1 Participant characteristics

After quality assurance exclusions (section 2.3), we studied 123 participants between the ages of 12 and 30 (*M* = 21.08, *SD* = 3.54, 70 females). Potential participants were also excluded for metallic implants, claustrophobia, pregnancy, acute intoxication, as well as significant medical and/or developmental conditions that would have impeded participation. All subjects were compensated for their time, and all protocols were approved by the University of Pennsylvania's Institutional Review Board.

2.2 Image acquisition

All participants were imaged on a 3-Tesla Siemens MAGNETOM Prisma with a T1-weighted structural and diffusion-weighted scan. Our structural scan was a 3 min 28 s sequence with 0.9 x 0.9 x 1.0 mm^3 resolution (TR = 1810 ms, TE = 3.45 ms, inversion time = 1100 ms, flip angle = 9 degrees, acceleration factor = 2). Our DWI sequence was a single-shot, multi-shell acquisition protocol (TR = 3027 ms, TE = 82.80 ms, flip angle = 78 degrees, voxel size = 1.5 mm^3 isotropic, FOV = 210 mm, acquisition time = 6 minutes 12 seconds, acceleration factor = 4, phase-encoding direction = anterior to posterior) with 3 diffusion-weighted shells at b=300 s/mm^2 (15 volumes), b=800 s/mm^2 (30 volumes), and b = 2000 s/mm^2 (64 volumes). The sequence included 9 b=0 s/mm^2 scans interspersed throughout. We also acquired a b=0 s/mm^2 reference scan with the opposite phase-encoding direction (posterior to anterior) to correct for phase-encoding direction-induced distortions.

2.3 Pre-processing and quality assurance

Distortions induced by phase encoding were corrected using *topup* from the FMRIB Software Library (*FSL*; Jenkinson et al., 2012). Eddy-current distortions and in-scanner movement were corrected using *eddy* from FSL version 5.0.11 with both single slice and multi-band outlier replacement (Jenkinson et al., 2012; Andersson et al., 2016). Following prior work, we quantified in-scanner motion using the root mean squared displacement over the course of the scan (mean relative RMS; Baum et al., 2018; Roalf et al., 2016). Mean relative RMS displacement was calculated between uncorrected interspersed b=0 images using publicly available scripts (https://www.med.upenn.edu/cmroi/qascripts.html). Following manual inspection of T1 images, one subject was removed for poor T1 image quality. Additionally, one subject was removed for poor DWI quality (motion + 6.92 *SD* above the mean). Motion, distortion, and eddy-corrected images served as the common input to all diffusion modeling techniques.

2.4 Overview of diffusion metrics of interest

We evaluated FA from DTI, ICVF from NODDI, and RTOP from MAPL (Basser, Mattiello, and Le Bihan 1994; Zhang et al., 2012; Fick et al., 2016). FA was selected because it is the most commonly used metric of diffusion. We selected ICVF because previous research has shown that it may have stronger associations with age than traditional diffusion metrics (Chang et al., 2015; Genc et al., 2017; Mah, Geeraert, and Lebel 2017). Finally, we evaluated RTOP over other MAPL metrics because RTOP does not require estimation of the underlying fiber geometry.

2.4.1 Fractional anisotropy

DTI assesses the directionality and magnitude of water diffusion by assuming a Gaussian diffusion process in each voxel. To this end, a 6 degrees of freedom symmetric tensor model is fit to the observed signal. Subsequently, the primary direction of diffusion in a voxel is calculated by finding the largest eigenvector of the tensor. After tensors are fit to a voxel in DTI, FA can be calculated. FA is the fraction of anisotropy in a voxel aligned with a primary direction of diffusion. As isotropic diffusion is the product of undirected, Brownian motion, the fraction of anisotropy is reflective of the degree of directional constraint upon diffusing molecules. The FA of a voxel is calculated as follows:

$$FA = \sqrt{\frac{3}{2}} \frac{\sqrt{(\lambda_1 - MD)^2 + (\lambda_2 - MD)^2 + (\lambda_3 - MD)^2}}{\sqrt{\lambda_1 + \lambda_2 + \lambda_3}}$$

where λ_{1-3} represents diffusion along 3 perpendicular eigenvectors in 3 dimensions, and MD is the mean diffusivity of the voxel, or average diffusion across the vectors. The factor $\sqrt{3/2}$ is a normalization constant, set to scale observations of fractional anisotropy between 0 (no net directionality of diffusion) and 1 (complete limitation of diffusion to one axis). As diffusion shows directional preference, the λ most closely corresponding to the over-represented direction increases beyond the mean diffusivity of a voxel. As a consequence, when a λ reflects increasing anisotropy, $(\lambda - MD)^2$ also grows, as does the numerator (Basser, Mattiello, and Le Bihan 1994).

FA was calculated in Camino (Cook et al., 2006). We used the *Wdtfit* procedure, a weighted linear tensor fitting method, as it has been shown to improve DTI estimations in protocols leveraging multiple *b*-values (Jones and Basser 2004; Veraart et al., 2013). To ensure that our results were not specific to this procedure, we also calculated FA using FSL's FMRIB's Diffusion Toolbox using a non-weighted linear fit (FDT; Jenkinson et al., 2012). Additionally, we evaluated FA using the *b* = 800 shell only, in case the utility of including more diffusion directions was outweighed by the non-Gaussian contribution of high *b*-value acquisitions. This shell was extracted and evaluated using MRtrix3 (Tournier et al., 2012). These two alternate methods of calculating FA were highly correlated with the weighted FA returned by Camino (*r*=0.94 and *r*=0.89, respectively), and were not evaluated further.

2.4.2 Intracellular volume-fraction

NODDI estimates the directional distribution of neurites (axons and dendrites) in a voxel, and then matches diffusion patterns to that distribution. Like DTI, this model is informed by hindrance of diffusion unaligned with neuronal fibers, and unhindered diffusion along their prominent axes. Unlike DTI, the introduction of a 3D neurite distribution allows for modeling diffusion restriction in fiber populations with dispersed orientations.

ICVF is derived from NODDI, which attempts to parse the diffusion signal into discrete contributions of cellular compartments. The total signal is set to equal the sum of the contributions from each compartment, such that $A = (1 - V_{iso})(V_{ic}A_{ic} + (1 - V_{ic})A_{ec}) + V_{iso}A_{iso}$, where A is the full diffusion signal, A_{ic}, A_{ec}, and A_{iso} are the signal attributable to the intracellular, extracellular, and isotropic compartments, and V_{iso}, V_{ic}, and V_{ec} represent the fraction of tissue volume attributable to the same compartments. In order to assign diffusion signal to one of these compartments, the method assumes neurites can be modeled as zero-radius cylinders, or sticks. NODDI then fits an estimated distribution of these sticks to a spherical distribution, and A_{ic} is calculated with respect to the posited orientation dispersion in any given voxel. Estimation of the intracellular signal is solved by comparing the spherical distribution of neurite orientations with the distribution of unimpeded diffusion. This calculation takes the form of $A_{ic} = \int_{S^2} f(\mathbf{n}) u d\mathbf{n}$, where $f(\boldsymbol{n})d\boldsymbol{n}$ indicates the probability of finding zero-radius cylinders along orientation $\mathbf{n}$, and u is the signal attenuation due to unhindered diffusion along the same orientation. Hindered and isotropic

diffusion signal are attributed to extracellular and cerebrospinal fluid compartments, respectively. Finally, after establishing the relative proportions of signal from each compartment, NODDI makes estimates of what fraction of each voxel belong to each compartment (Zhang et al., 2012). This fraction is then referred to as a volume fraction. Recent advances have markedly accelerated fitting the NODDI model; here we calculated ICVF using AMICO (Daducci et al., 2015).

2.4.3 Return-to-origin probability

Unlike tissue based models such as NODDI, signal-based techniques which seek to model the EAP directly do not assume the separability of specific tissue compartments. Notably, the EAP is not limited to representing ellipsoids, and can therefore in theory capture arbitrary fiber configurations. MAP-MRI expresses MR signal utilizing Hermite functions as a basis set, which allows for rapid convergence of function solutions (Walter 1977). Building on MAP-MRI, Fick et al., (2016) recently introduced Laplacian-regularized MAP-MRI (MAPL). MAPL imposes additional smoothness on MAP-MRI's coefficient estimation using the norm of the Laplacian of the reconstructed signal. This approach effectively penalizes model fits with physiologically inaccurate high local variances, which are more likely to be artifactual than signals of interest (Descoteaux et al., 2007). The authors also demonstrated that this method reduces error over MAP-MRI in voxels with crossing fibers (Fick et al., 2016).

Return to origin probability (RTOP) is an EAP-based anisotropy index that indicates the likelihood of diffusing molecules undergoing zero net displacement. The primary computation involved in MAPL represents the observed diffusion signal in terms of Hermite functions. After this fit is made, diffusion metrics are calculated. RTOP is defined as $\int_{\mathrm{R}^3} E(\mathbf{q}) d(\mathbf{q})$, where $\boldsymbol{q}$ is a controlled parameter that incorporates duration, magnitude and direction of the diffusion sensitizing gradients in a scanning protocol (Stejskal and Tanner 1965), and $E(\boldsymbol{q})$ is the ratio of the signal at $\boldsymbol{q}$ to $\boldsymbol{q} = 0$ (non-diffusion weighted acquisitions; Özarslan et al., 2013). We generated RTOP with dmipy, an open-source diffusion microstructure toolbox in Python (Fick, Deriche, and Wassermann 2018; Alimi et al., 2018).

2.6 Structural Image Processing

T1 images were processed using the ANTs Cortical Thickness Pipeline (Tustison et al., 2014). Images were bias field corrected using N4ITK (Tustison et al., 2010), and brains were extracted from T1 images using study-specific tissue priors (Avants, Tustison, Wu, et al., 2011). We utilized a custom young-adult template constructed via the *buildtemplateparallel* procedure in ANTs (Avants, Tustison, Song, et al., 2011). A custom template was used due to evidence demonstrating the utility of custom templates in reducing registration biases (Tustison et al., 2014). The T1 to template affine and diffeomorphic transformations were calculated with the top-performing symmetric diffeomorphic normalization (SyN) tool in ANTs (Klein et al., 2009). The transforms between T1 and the initial b=0 DWI images were calculated using boundary-based registration with 6 degrees of freedom (Greve and Fischl 2009). All transforms were concatenated so that only one interpolation was performed.

2.7 Network construction

Accumulating evidence suggests that structural brain networks undergo substantial maturation during youth (Hagmann et al., 2010; Fan et al., 2011; Grayson et al., 2014; Baum et al., 2017; Uddin et al., 2011; Baker et al., 2015). Accordingly, in addition to analysis of summary measures and scalar maps, we evaluated each measure in the context of a network. Subject brains were divided into network nodes using the Schaefer 200 cortical parcellation (Schaefer et al., 2014). The parcellation was warped to the custom template, and then projected back to each subject's T1 and native

diffusion space using the inverse of each transform. Whole-brain connectomes were constructed by representing each of the 200 regions as a network node, and by representing deterministic tractography streamlines as network edges. Tractography was conducted in Camino (Cook et al., 2006) using the Euler tracking algorithm in native diffusion space (Basser et al., 2000). The boundary between gray and 1mm-dilated white matter was used as both seed regions and termination points for tractography. We used voxels defined as CSF by the segmented T1 image as termination boundaries for streamlines. Voxels defined as white matter by the segmented T1 image were used as an inclusion mask for streamlines, ensuring that streamlines had to pass through white matter. Additionally, we imposed a curvature restriction on all streamlines. Fibers determined to curve more than 60 degrees over a 5 millimeter interval were discarded in order to mitigate the impact of noise on tractography (Bastiani et al., 2012). Lastly, the mean FA, ICVF, and RTOP were calculated along each edge in this network. These values were used as edge weights between nodes connected via tractography streamlines.

2.8 Statistical analyses

Within subjects, Spearman's ρ between each diffusion metric for all white matter voxels was calculated. This involved masking diffusion images, vectorizing scalar values for each voxel, and correlating the vectors for each image. Subsequent analyses utilized consistent models across three levels of features (see schematic in **Figure 1**). First, we compared mean values within a white matter mask. Second, we conducted mass-univariate voxelwise analyses within white matter. Third, we evaluated tractography-based structural networks. At each level, in order to rigorously model linear and nonlinear associations with age, we used generalized additive models (GAMs; Wood, 2001, 2004) with penalized splines in R (Version 3.5.1) using the *mgcv* package (R Development Core Team, 2010; Wood, 2011). To avoid over-fitting, nonlinearity was penalized using restricted maximum likelihood (REML). Age was modeled as a penalized spline; sex and in-scanner motion were included as linear effects. For in-scanner motion relations, the residuals from these models were utilized to provide an estimate of effect sizes. Type I error was accounted for using the False Discovery Rate (FDR; $Q<0.05$).

2.9 Data and code availability

Data acquisition from this study is ongoing and will be made available upon completion. All analysis code used is available at: github.com/PennBBL/multishell_diffusion.

3. RESULTS

3.1 Relationships between measures

As an initial step, we investigated the relationships between FA and both ICVF and RTOP (**Figure 2**). Across subjects, the average correlation between FA and ICVF was 0.670 (SD = 0.040). FA and RTOP were also correlated (r = 0.732 SD = 0.037), and ICVF and RTOP had an average correlation of 0.735 (SD = 0.047). Next, we sought to differentiate diffusion metrics in terms of their relationship to neurodevelopment.

3.2 White matter ICVF and RTOP are more associated with age than FA

Next, we evaluated the degree to which each scalar metric of restricted diffusion associated with age. Both mean white matter values and high-resolution mass-univariate analyses at each voxel were conducted. Mean white matter values were related to age in our sample (**Figure 3A & B**). However, while controlling for sex and motion, mean FA in white matter was only weakly associated with age (F = 3.267, p = 0.041). In contrast, ICVF (F = 14.13, p = 3.58×10^{-7}) and RTOP (F = 12.66, p = 8.00×10^{-7}) were more strongly associated with age. Voxelwise analyses within white

matter revealed a similar pattern. Specifically, only two voxels were significantly associated with age for FA after FDR correction. However, 15,231 voxels demonstrated statistically significant associations with age for ICVF, while 11,382 voxels were associated with age for RTOP (**Figure 3C**).

3.3 ICVF and RTOP are more associated with structural network development

Given that tools from network science are increasingly used to study the developing brain, we next evaluated associations with age within networks where edges were either weighted by FA, ICVF, or RTOP. These analyses yielded similar results as the voxelwise analyses described above, with both ICVF and RTOP displaying more widespread associations with age than FA. Specifically, 80 edges were significantly (Q<0.05) related to age within FA-weighted networks. In contrast, there were 418 edges that were significantly associated with age within ICVF-weighted networks, and 321 significant edges within RTOP-weighted networks (**Figure 4**).

3.4 Mean ICVF and RTOP are less impacted by in-scanner motion than FA

As a final step, we sought to characterize the impact of motion on all three diffusion models. Evaluation of mean white matter values of FA, ICVF, and RTOP revealed that FA was more strongly related to motion than ICVF or RTOP (**Figure 5**). Specifically, head motion was significantly associated with mean FA (p = 0.004, r = -0.255), but not ICVF (p = 0.242, r = 0.103) or RTOP (p = 0.563, r = 0.050) when controlling for age and sex. However, associations with motion were not widespread after correction for multiple comparisons in voxelwise or network analyses. After FDR correction, less than 10 voxels were significantly associated with motion for FA, ICVF, and RTOP. Similarly, analyses of networks weighted by each of these values revealed that less than 25 edges were associated with head motion for all three measures.

4. DISCUSSION

Our findings suggest that diffusion models leveraging multi-shell data have important advantages for studying the developing brain. ICVF and RTOP were much more strongly associated with age than FA at multiple scales, including mean white matter values, voxelwise analyses, and network edges. Furthermore, multi-shell measures of microstructure were less impacted by motion on a global level. Taken together, these results emphasize the relative utility of multi-shell diffusion models for studies of brain development.

4.1 ICVF and RTOP demonstrate superior sensitivity to brain development

In our dataset, FA was weakly related to age across white matter, whereas ICVF and RTOP had stronger associations. These results advance previous findings in several respects. First, to our knowledge, this is the first study to demonstrate that RTOP from MAPL is highly sensitive to brain development in youth. This is potentially important, as the absence of fixed tissue parameters in signal-based models of the EAP such as MAPL may confer advantages over NODDI (Karmacharya et al., 2018; Rensonnet et al., 2019). Second, our results demonstrate that multi-shell measures of structural brain network connectivity such as ICVF and RTOP are more strongly associated with age than traditional FA-weighted networks. This result builds upon prior regional or voxelwise analyses, which have shown that ICVF from NODDI is more strongly associated with age than FA (Chang et al., 2015; Genc et al., 2017; Ota et al., 2017). Overall, these results emphasize the utility of multi-shell modeling techniques for studying brain development. These advantages of multi-shell models likely stem from their ability to successfully capture the evolution of complex white matter architecture during development, including crossing fibers (Jeurissen et al., 2013; Volz, Cieslak, and Grafton 2018) and dispersed fiber orientations (Zhang et al., 2012).

4.2 ICVF and RTOP are less impacted by head motion than FA

Importantly, higher in-scanner motion was associated with reduced mean white matter FA while accounting for age. This finding aligns with prior reports of in-scanner motion systematically reducing FA (Yendiki et al., 2014; Ling et al., 2012, Roalf et al., 2016; Baum et al., 2018). As for other imaging modalities, the primary determinant of scan quality for diffusion imaging is in-scanner head motion (Yendiki et al., 2014; Ling et al., 2012). Because younger children are more likely to have difficulties with motion than adults, motion artifact is a major concern for studies of brain development (Theys, Wouters, & Ghesquière, 2014; Satterthwaite et al., 2013; Fair et al., 2012). Motion has several effects on the diffusion image. First, unaddressed head displacement alters the region from which a voxel is being acquired in the brain. Second, head rotations change the observed orientations of diffusion in the brain. Third, movement can bring previously excited tissue back into the acquisition plane, which results in lower signal due to incomplete relaxation (Friston et al., 1996).

In comparison to FA, ICVF and RTOP had a more attenuated relationship with motion. Importantly, these models were fit from the same distortion-corrected diffusion images. This may be due to the fact that NODDI and MAPL incorporate local differences in signal decay rates across *b*-values into their measurements of diffusion restriction. Although more intricate, such techniques may be less impacted by head rotations than measurements (such as FA) that are entirely based on identifying the primary direction of diffusion. Especially for studies of brain development, where motion can be a major confound, these advantages are particularly notable when considered together with the observed increase in associations with age.

4.3 Limitations and future work

Several limitations should be noted. First, our results were only derived from one protocol. Replication of these results in other multi-shell protocols would strengthen evidence for the relative advantages of multi-shell models. Second, our study only evaluated adolescents and young adults. Studies of younger children would provide complimentary data, as white matter may undergo even more dramatic microstructural changes at earlier ages (Lebel et al., 2008). Third, it should be noted that compared to prior studies (Roalf et al., 2016, Yendiki et al., 2014, Baum et al., 2018), we detected a relative paucity of relationships between FA and motion. This may be due to both advances in diffusion image processing techniques (such as the outlier replacement implemented in FSL's *eddy*) and reduced statistical power. While the sample size of the present study is not small, it is a fraction of the size of other recent reports that evaluated the impact of motion on single-shell acquisitions (Baum et al., 2018, Roalf et al., 2016). Fourth, we used deterministic DTI-based tractography to define the streamlines, which results in a sparse structural network biased towards major white matter tracts. While these network analyses demonstrated enhanced associations with both NODDI and MAPL, networks constructed using multi-fiber tractography techniques might provide additional advantages (Maier-Hein et al., 2017; Reddy & Rathi, 2016; Farooq et al., 2016; Christiaens et al., 2015; Boniha et al., 2015).

4.4. Conclusion

In summary, across multiple levels of analysis, we found that ICVF (from NODDI) and RTOP (from MAPL) were associated with age in youth more than DTI-derived FA. Additionally, use of ICVF or RTOP mitigated the confounding impact of head motion. Given these advantages, multi-shell measures of microstructure are likely to be particularly useful for developmental or clinical samples. Through free open-access software, these advanced diffusion methods are relatively easy for investigators to implement (Alimi et al., 2018; Daducci et al., 2015; Fick, Deriche, and Wassermann 2018; Garyfallidis et al., 2014). In the context of these results, we anticipate that

multi-shell diffusion models will be increasingly adopted by the developmental and clinical neuroscience community.

ACKNOWLEDGEMENTS: This work was supported by grants from the National Institute of Mental Health: R01MH107703, R01MH113550, R01MH112847, R21MH106799, RF1MH116920, and F31 MH115709. Additional support was provided by the AE Foundation, the Center for Biomedical Computing and Image Analysis (CBICA) at Penn, and the Penn/CHOP Lifespan Brain Institute.

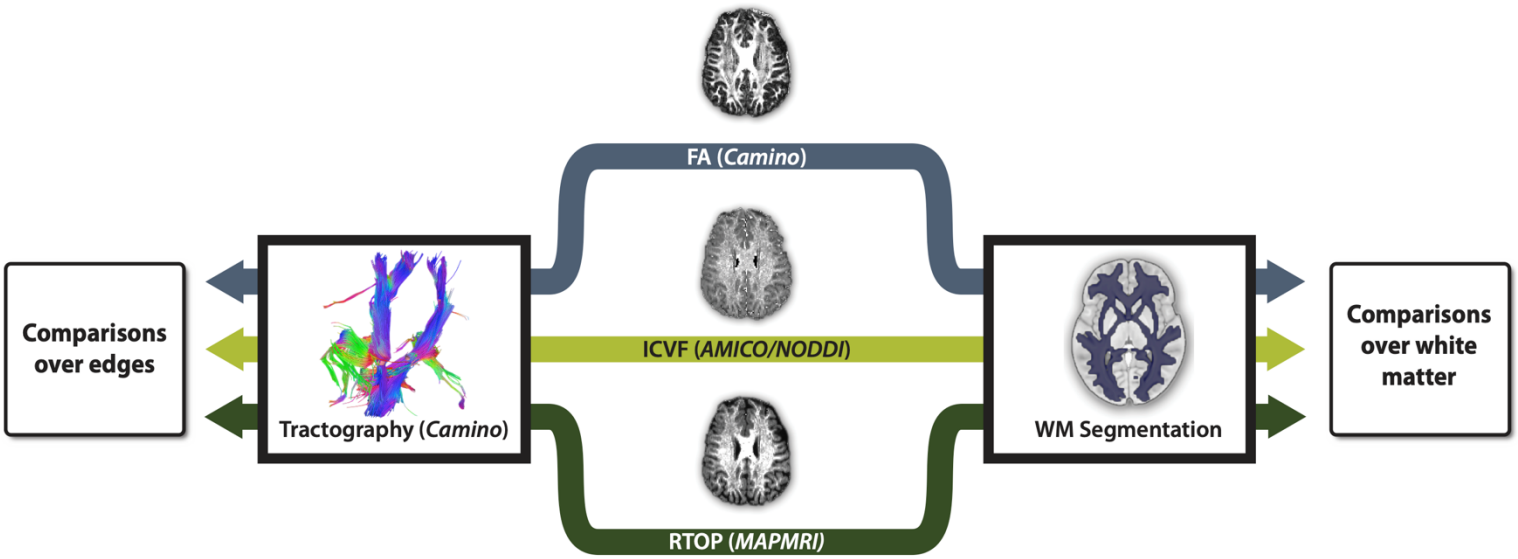

Figure 1: Data processing workflow**.** Scalar maps for FA, ICVF, and RTOP were derived from the same motion, distortion, and eddy-current corrected images. These maps were evaluated for associations with both age and data quality at multiple scales. Analyses evaluated mean white matter values, mass-univariate voxelwise analyses, and analyses of network edges reconstructed by deterministic tractography (and then weighted by each measure).

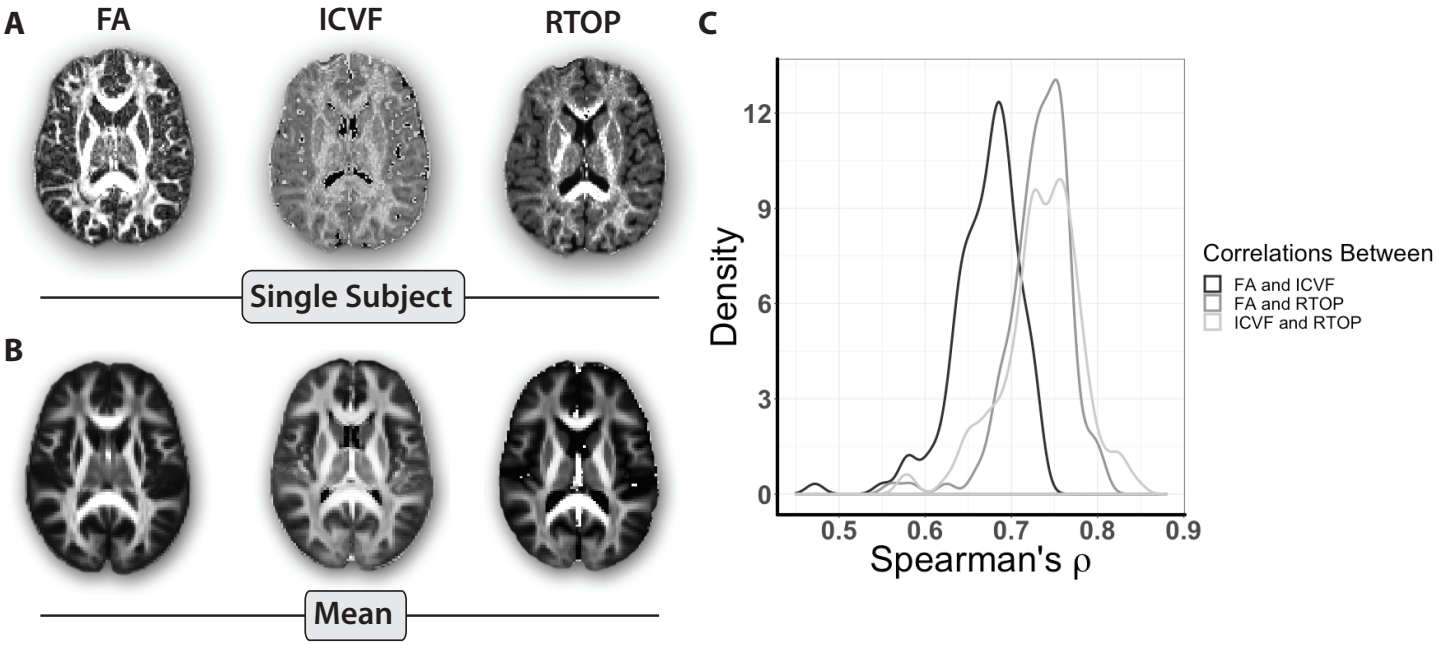

Figure 2: Sample scalar maps and correlations between measures. Axial slices of each scalar map from a single participant (**A**) and the average of all participants (**B**). Distributions of Spearman's correlations between FA, ICVF, and RTOP within white matter (**C**).

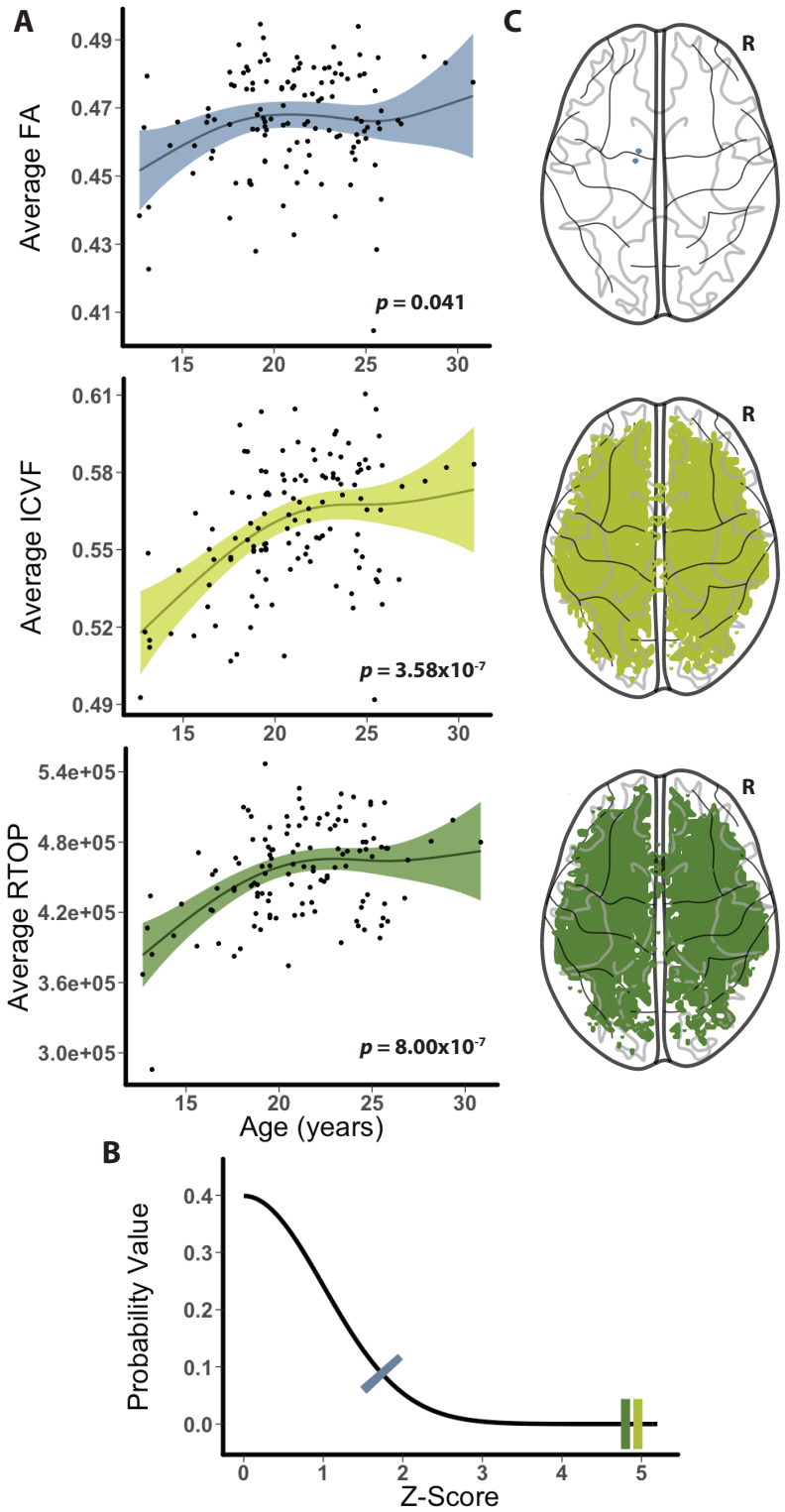

Figure 3: ICVF and RTOP show increased associations with age in white matter compared to FA. **A**: Generalized additive models (GAMs) of the mean value of each metric in standard-space white matter by age, with head motion and sex included as linear covariates. FA was less associated with age than ICVF and RTOP. **B**: Visualization of significance values derived from GAMs in panel **A** on a normal distribution. **C**: Mass-univariate voxelwise analyses of standard space scalar maps. All depicted voxels were significant for linear or non-linear age effects after FDR-correction ($Q < 0.05$). Associations with age were significant in 2 voxels for FA, 15,231 voxels for ICVF, and 11,382 voxels for RTOP.

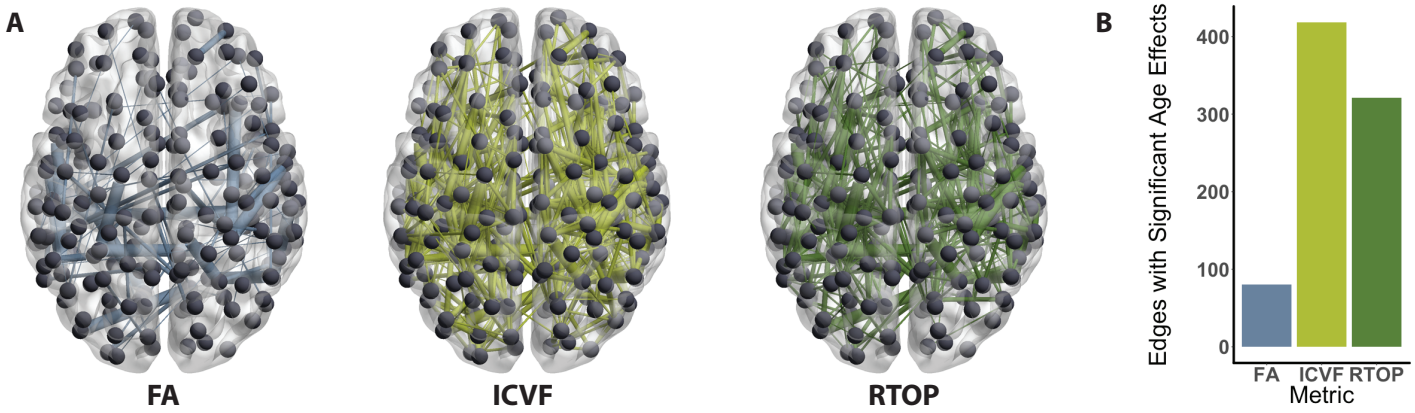

Figure 4: ICVF- and RTOP-weighted networks show increased associations with age compared to FA-weighted networks. **A**: Edges that displayed significant associations with following FDR-correction ($Q < 0.05$), while controlling for sex and head motion. Thickness of edges is scaled to their z-transformed *p*-values, with lower *p*-values depicted by thicker edges. **B**: Number of network edges significantly associated with age, by edge weight.

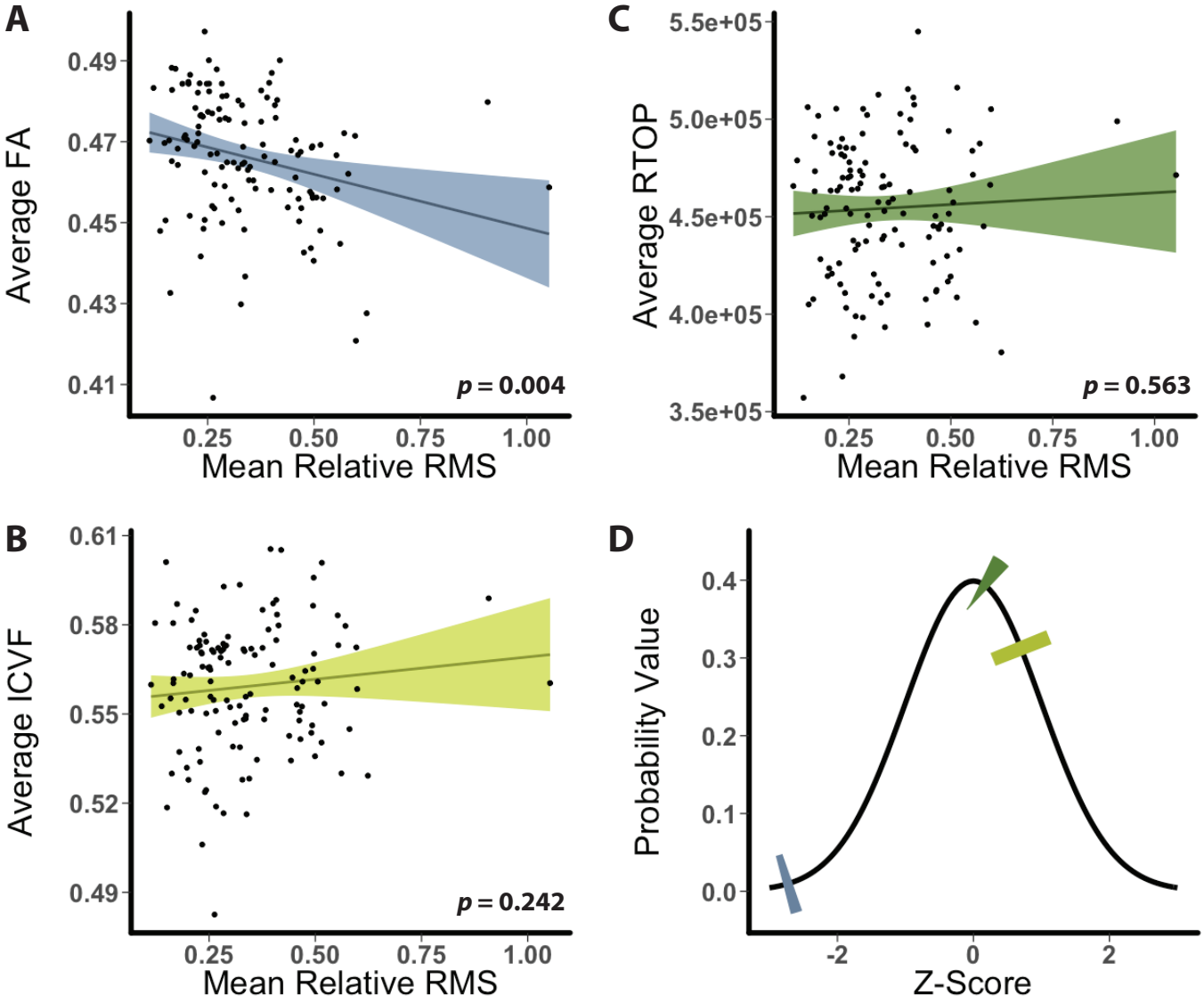

Figure 5: Compared to FA, ICVF and RTOP show diminished association with head motion. **A-C**: Associations between each metric and in-scanner motion, after controlling for sex and age. Whereas mean white matter FA was lower in participants with more head motion, ICVF and RTOP did not demonstrate a significant relationship with motion. **D**: Visualization of significance values (from panels **A-C**) on a normal distribution.

REFERENCES

Alexander, D.C., Dyrby, T.B., Nilsson, M., Zhang, H. 2017., Imaging Brain Microstructure with Diffusion Mri: Practicality and Applications. NMR in Biomedicine.

Alexander, D.C., Hubbard P.L., Hall, M.G., Moore, E.A., Ptito, M., Parker, G.J.M., Dyrby, T.B., 2010. Orientationally Invariant Indices of Axon Diameter and Density from Diffusion Mri. NeuroImage 52 (4): 1374–89.

Alimi, A., Fick, R., Wassermann, D., Deriche, R., 2018. Dmipy, a Diffusion Microstructure Imaging Toolbox in Python to Improve Research Reproducibility. In https://hal.inria.fr/hal-01873353/document.

Andersson, J.L.R., Graham, M.S., Zsoldos, E., Sotiropoulos, S.N., 2016. Incorporating Outlier Detection and Replacement into a Non-Parametric Framework for Movement and Distortion Correction of Diffusion MR Images. NeuroImage 141, 556–72.

Andersson, J.L.R., Graham, M.S., Drobnjak, I., Zhang, H., Filippini, N., Bastiani, M., 2017. Towards a Comprehensive Framework for Movement and Distortion Correction of Diffusion MR Images: Within Volume Movement. Neuroimage 152, 450–66.

Assaf, Y., Basser, P.J., 2005. Composite Hindered and Restricted Model of Diffusion (Charmed) MR Imaging of the Human Brain. NeuroImage 27 (1), 48–58.

Assaf, Y., Ofer P., 2008. Diffusion Tensor Imaging (DTI)-Based White Matter Mapping in Brain Research: A Review. Journal of Molecular Neuroscience 34 (1), 51–61.

Avants, B.B., Tustison, N.J., Song, G., Cook, P.A., Klein, A., Gee, J.C., 2011. A Reproducible Evaluation of Ants Similarity Metric Performance in Brain Image Registration. NeuroImage 54 (3), 2033–44.

Avants, B.B., Tustison, N.J, Wu, J., Cook, P.A., Gee, J.C., 2011. Neuroinformatics 9 (4), 381–400. Baker, S.T.E., Lubman, D.I., Yücel, M., Allen, N.B., Whittle, S., Fulcher, B.D., Zalesky, A., Fornito, A., 2015. Developmental Changes in Brain Network Hub Connectivity in Late Adolescence. Journal of Neuroscience 35 (24), 9078–87.

Basser, P.J., Pierpaoli, C., 1996. Microstructural and Physiological Features of Tissues Elucidated by Quantitative-Diffusion-Tensor MRI. Journal of Magnetic Resonance. Series B 111 (3), 209–19.

Basser, P.J., Mattiello, J., Le Bihan, D., 1994. MR Diffusion Tensor Spectroscopy and Imaging. Biophysical Journal 66 (1), 259–67.

Basser, P.J., Pajevic, S., Pierpaoli, C., Duda, J., Aldroubi, A., 2000. In Vivo Fiber Tractography Using DT-MRI Data. Magnetic Resonance in Medicine 44 (4), 625–32.

Bassett, D.S., Zurn, P., & Gold, J.I., 2018. On the nature and use of models in network neuroscience. Nature Reviews Neuroscience 19 (9) , 566.

Bastiani, M., Shah, N.J., Goebel, R., Roebroeck, A., 2012. Human cortical connectome reconstruction from diffusion weighted MRI: The effect of tractography algorithm. NeuroImage,62(3), 1732–1749.

Baum, G.L., Ciric, R., Roalf, D.R., Betzel, R.F., Moore, T.M., Shinohara, R.T., Kahn, A.E., Vandekar, S.N., Rupert., P.E., Quarmley, M., Cook, P.A., Elliott, M.A., Ruparel, K., Gur., R.E., Gur, R.C., Bassett, D.S., Satterthwaite., T.D., 2017. Modular Segregation of Structural Brain Networks Supports the Development of Executive Function in Youth. Current Biology 27 (11), 1561–1572

Baum, G.L., Roalf, D.R., Cook, P.A., Ciric, R., Rosen, A.F.G., Xia, C., Elliott, M.A., Ruparel, K., Verma, R., Tunç, B., Gur, R.C., Gur, R.E., Bassett., D.S., Satterthwaite., T.D., 2018. The Impact of in-Scanner Head Motion on Structural Connectivity Derived from Diffusion MRI. NeuroImage 173, 275–86.

Bonilha, L., Gleichgerrcht, E., Fridriksson, J., Rorden, C., Breedlove, J.L., Nesland, T., Paulus, W., Helms, G., Focke, N.K., 2015. Reproducibility of the Structural Brain Connectome Derived from Diffusion Tensor Imaging. PLOS ONE 10 (9), e0135247.

Chang, Y.S., Owen, J.P., Pojman, N.J., Thieu, T., Bukshpun, P., Wakahiro, M.L.J., Berman, J.I., 2015. White Matter Changes of Neurite Density and Fiber Orientation Dispersion During Human Brain Maturation. PLOS ONE 10 (6): e0123656.

Clark, C.A., Le Bihan., D., 2000. Water Diffusion Compartmentation and Anisotropy at High B Values in the Human Brain. Magnetic Resonance in Medicine 44 (6), 852–59.

Clark, C.A., Hedehus, M., Moseley, M.E., 2002. In Vivo Mapping of the Fast and Slow Diffusion Tensors in Human Brain. Magnetic Resonance in Medicine 47 (4), 623–28.

Cook, P.A., Bai, Y., Nedjati-Gilani, S., Seunarine, K.K., Hall, M.G., Parker, G.J., Alexander, D.C., 2006. Camino: Open-Source Diffusion-Mri Reconstruction and Processing, 14th Scientific Meeting of the International Society for Magnetic Resonance in Medicine, Seattle, WA, USA, p. 2759.

Cook, P.A., Alexander, D.C., Parker, G.J.M., 2004. Modelling Noise-Induced Fibre-Orientation Error in Diffusion-Tensor MRI. In 2004 2nd IEEE International Symposium on Biomedical Imaging: Nano to Macro (1), 332–35

Christiaens D., Reisert M., Dhollander T., Sunaert S., Suetens P., Maes F., 2015 Global tractography of multi-shell diffusion-weighted imaging data using a multi-tissue model. Neuroimage 123, 89–101.

Daducci, A., Canales-Rodríguez, E.J., Zhang, H., Dyrby, T.B., Alexander, D.C., Thiran, J.P., 2015. Accelerated Microstructure Imaging via Convex Optimization (Amico) from Diffusion Mri Data. NeuroImage 105, 32–44.

Deligianni, F., Carmichael, D.W., Zhang, H., Clark, C.A., Clayden, J.D., 2016. NODDI and Tensor-Based Microstructural Indices as Predictors of Functional Connectivity. PLOS ONE 11 (4): e0153404.

Descoteaux, M., Angelino, E., Fitzgibbons, S., Deriche, R., 2007. Regularized, fast, and robust analytical q-ball imaging. Magnetic Resonance in Medicine 58 (3), 497–510.

Douek, P., Turner, R., Pekar, J., Patronas, N., Le Bihan, D., 1991. MR Color Mapping of Myelin Fiber Orientation. Journal of Computer Assisted Tomography 15 (6), 923–29.

Fair, D.A., Nigg, J.T., Iyer, S., Bathula, D.R., Mills, K.L., Dosenbach, N.U.F., Schlaggar, B.L., Mennes, M., Gutman, D., Bangaru, S., Buitelaar, J.K., Dickstein, D.P., Di Martino, A., Kennedy, D.N., Kelly, C., Luna, B., Schweitzer, J.B., Velanova, K., Wang, Y.-F., Mostofsky, S., Castellanos, X.F., Milham, M.P., 2012. Distinct neural signatures detected for ADHD subtypes after controlling for micro-movements in resting state functional connectivity MRI data. Frontiers in Systems Neuroscience 6, 80.

Eaton-Rosen, Z., Melbourne, A., Orasanu, E., Cardoso, M.J., Modat, M., Bainbridge, A., Kendall, G.S., Robertson, N.J., Marlow, N., Ourselin, S., 2015. Longitudinal Measurement of the Developing Grey Matter in Preterm Subjects Using Multi-Modal MRI. NeuroImage 111, 580–89.

Fan, Y., Shi, F., Smith, J.K., Lin, W., Gilmore, J.H., Shen, D., 2011. Brain Anatomical Networks in Early Human Brain Development. NeuroImage 54 (3), 1862–71.

Farooq, H., Xu, J., Nam, J.W., Keefe, D.F., Yacoub, E., Georgiou, T., Lenglet, C., 2016. Microstructure imaging of crossing (MIX) white matter fibers from diffusion MRI. Scientific Reports 6, 38927.

Ferizi, U., Scherrer, B., Schneider, T., Alipoor, M., Eufracio, O., Fick, R.H.J., Deriche, R., Nilsson, M., Loya-Olivas, A.K., Rivera, M., Poot, D.H.J., Ramirez-Manzanares, A., Marroquin, J.L., Rokem, A., Pötter, C., Dougherty, R.F., Sakaie, K., Wheeler-Kingshott, C., Warfield, S.K., Witzel, T., Wald, L.L., Raya, J.G., Alexander, D.C., 2017. Diffusion Mri Microstructure Models with in Vivo Human Brain Connectome Data: Results from a Multi-Group Comparison. NMR in Biomedicine 30 (9).

Fick, R.H.J., Wassermann D., Caruyer E., Deriche, R., 2016. MAPL: Tissue Microstructure Estimation Using Laplacian-Regularized MAP-MRI and Its Application to HCP Data. NeuroImage 134, 365–85.

Fick, R.H.J., Deriche, R, Wassermann, D., 2018. Dmipy: An Open-source Framework for Reproducible dMRI-Based Microstructure Research (Version 0.1). Zenodo.

Friston, K.J., Williams, S., Howard, R., Frackowiak, R.S.J, Turner, R., 1996. Movement-Related Effects in fMRI Time-Series. Magnetic Resonance in Medicine 35 (3), 346–55.

Garyfallidis, E., Brett, M., Amirbekian, B., Rokem, A., Van Der Walt, S., Descoteaux, M., Nimmo-Smith, I., 2014. Dipy, a Library for the Analysis of Diffusion MRI Data. Frontiers in Neuroinformatics 8.

Genc, S., Malpas, C.B., Holland, S.K., Beare, R., Silk, T.J., 2017. Neurite Density Index Is Sensitive to Age Related Differences in the Developing Brain. NeuroImage 148, 373–80.

Gollo, L.L., Roberts, J.A., Cropley, V.L., Di Biase, M.A., Pantelis, C., Zalesky, A, Breakspear, M., 2018. Fragility and Volatility of Structural Hubs in the Human Connectome. Nature Neuroscience 21 (8), 1107.

Grayson, D.S., Ray S., Carpenter, S., Swathi Iyer, Dias, T.C.G., Stevens, C., Nigg, J.T., Fair, D.A., 2014. Structural and Functional Rich Club Organization of the Brain in Children and Adults. PLOS ONE 9 (2), e88297.

Greene, D.J., Black, K.J., Schlaggar, B.L., 2016. Considerations for MRI Study Design and Implementation in Pediatric and Clinical Populations. Developmental Cognitive Neuroscience, Flux congress 2014, 18 (April), 101–12.

Greve, D.N., Fischl, B., 2009. Accurate and Robust Brain Image Alignment Using Boundary-Based Registration. NeuroImage 48 (1), 63–72.

Hagmann, P., Sporns, O., Madan N., Cammoun, L., Pienaar, R., Wedeen, V.J., Meuli, R., Thiran, J.P., Grant, P.E., 2010. White Matter Maturation Reshapes Structural Connectivity in the Late Developing Human Brain. Proceedings of the National Academy of Sciences of the United States of America 107 (44), 19067–72.

Huang, H., Shu, N., Mishra, V., Jeon, T., Chalak, L., Wang, Z.J., Rollins, N., Gong, G., Cheng, H., Peng, Y., Dong, Q., He, Y., 2015. Development of Human Brain Structural Networks Through Infancy and Childhood. Cerebral Cortex 25 (5), 1389–1404.

Jenkinson, M., Beckmann, C.F., Behrens, T.E.J., Woolrich, M.W., Smith, S.M., 2012. FSL. NeuroImage, 62 (2), 782–90.

Jeurissen, B., Leemans, A., Tournier, J., Jones, D.K., Sijbers, J., 2013. Investigating the Prevalence of Complex Fiber Configurations in White Matter Tissue with Diffusion Magnetic Resonance Imaging. Human Brain Mapping 34 (11), 2747–66.

Jones, D.K., Basser, P.J., 2004. 'Squashing Peanuts and Smashing Pumpkins': How Noise Distorts Diffusion-Weighted MR Data. Magnetic Resonance in Medicine 52 (5), 979–93.

Jones, D.K., Cercignani, M., 2010. Twenty-Five Pitfalls in the Analysis of Diffusion MRI Data. NMR in Biomedicine 23, 803–20.

Karmacharya, S., Gagoski, B., Ning, L., Vyas, R., Cheng, H.H., Soul, J., Newberger, J.W., Shenton, M.E., Rathi, Y., Grant, P.E., 2018. Advanced Diffusion Imaging for Assessing Normal White Matter Development in Neonates and Characterizing Aberrant Development in Congenital Heart Disease. Neuroimage: Clinical 19, 360–373.

Klein, A., Andersson, J., Ardekani, B.A., Ashburner, J., Avants, B., Chiang, M., Christensen, G.E., Collins, D.L., Gee, J., Hellier, P., Song, J.H., Jenkinson, M., Lepage, C., Rueckert, D., Thompson, P., Vercauteren, T., Woods, R.P., Mann, J.J., Parsey, R.V., 2009. Evaluation of 14 Nonlinear Deformation Algorithms Applied to Human Brain MRI Registration. NeuroImage 46 (3), 786–802.

Kodiweera, C., Alexander, A.L., Harezlak, J., McAllister, T.W., Wu, Y.C., 2016. Age Effects and Sex Differences in Human Brain White Matter of Young to Middle-Aged Adults: A DTI, NODDI, and Q-Space Study. NeuroImage 128, 180–92.

Koh, D.M., Padhani, A.R., 2006. Diffusion-Weighted MRI: A New Functional Clinical Technique for Tumour Imaging. The British Journal of Radiology 79 (944), 633–35.

Lebel, C., Deoni, S., 2018. The development of brain white matter microstructure. NeuroImage 182, 207-218.

Lebel, C., Treit, S., Beaulieu, C., 2017. A review of diffusion MRI of typical white matter development from early childhood to young adulthood. NMR in Biomedicine, e3778.

Lebel, C., Walker, L., Leemans, A., Phillips, L., Beaulieu, C., 2008. Microstructural Maturation of the Human Brain from Childhood to Adulthood. NeuroImage 40 (3), 1044–55.

Lerch, J.P., van der Kouwe, A.J.W., Raznahan, A., Paus, T., Johansen-Berg, H., Miller, K.L, Smith, S.M., Fischl, B., Sotiropoulos, S.N., 2017. Studying Neuroanatomy Using MRI. Nature Neuroscience 20 (3), 314–26.

Ling, J., Merideth, F., Caprihan, A., Pena, A., Teshiba, T., Mayer, A.R., 2012. Head Injury or Head Motion? Assessment and Quantification of Motion Artifacts in Diffusion Tensor Imaging Studies. Human Brain Mapping 33 (1), 50–62.

Mah, A., Geeraert, B., Lebel, C., 2017. Detailing Neuroanatomical Development in Late Childhood and Early Adolescence Using NODDI. PLOS ONE 12 (8), e0182340.

Maier-Hein, K.H., Neher, P.F., Houde, J.C., Côté, M.A., Garyfallidis, E., Zhong, J., Chamberland, M., Yeh, F.C., Lin, Y.C., Ji, Q., Reddick, W.E., Glass, J.O., Chen, D.Q., Feng, Y., Gao, C., Wu, Y., Ma, J., Renjie, H., Li, Q., Westin, C.F., Deslauriers-Gauthier, S., González, J.O.O., Paquette, M., St-Jean, S., Girard, G., Rheault, F., Sidhu, J., Tax, C.M.W., Guo, F., Mesri, H.Y., Dávid, S., Froeling, M., Heemskerk, A.M., Leemans, A., Boré, A., Pinsard, B., Bedetti, C., Desrosiers, M., Brambati, S., Doyon, J., Sarica, A., Vasta, R., Cerasa, A., Quattrone, A., Yeatman, J., Khan, A.R., Hodges, W., Alexander, S., Romascano, D., Barakovic, M., Auría, A., Esteban, O., Lemkaddem, A., Thiran, J.P., Cetingul, H.E., Odry, B.L., Mailhe, B., Nadar, M.S., Pizzagalli, F., Prasad, G., Villalon-Reina, J.E., Galvis, J., Thompson, P.M., Requejo, F.D.S., Laguna, P.L., Lacerda, L.M., Barrett, R., Dell'Acqua, F., Catani, M., Petit, L., Caruyer, E., Daducci, A., Dyrby, T.B., Holland-Letz, T., Hilgetag, C.C., Stieltjes, B., Descoteaux, M., 2017. The challenge of mapping the human connectome based on diffusion tractography. Nat. Communications 8, 1349.

Nazeri, A., Chakravarty, M.M., Rotenberg, D.J., Rajji, T.K., Rathi, Y., Michailovich, O.V., Voineskos, A.N., 2015. Functional Consequences of Neurite Orientation Dispersion and Density in Humans Across the Adult Lifespan. The Journal of Neuroscience: The Official Journal of the Society for Neuroscience 35 (4), 1753–62.

Ning, L., Westin, C., Rathi, Y., 2015. Estimating Diffusion Propagator and Its Moments Using Directional Radial Basis Functions. IEEE Transactions on Medical Imaging 34 (10), 2058–78.

Ota, M., Sato, N., Maikusa, N., Sone, D., Matsuda, H., Kunugi, H., 2017. Whole Brain Analyses of Age-Related Microstructural Changes Quantified Using Different Diffusional Magnetic Resonance Imaging Methods. Japanese Journal of Radiology, 1–6.

R Core Team (2013). R: A language and environment for statistical computing. R Foundation for Statistical Computing, Vienna, Austria. URL http://www.R-project.org/.

Reddy, C.P., Rathi, Y., 2016. Joint multi-fiber NODDI parameter estimation and tractography using the unscented information filter. Frontiers in Neuroscience 10, 1662-4548.

Rensonnet, G., Scherrer, B., Girard, G., Jankovski, A., Warfield, S.K., Macq, B., Thiran, J.P., Taquet. M., 2019. Towards Microstructure Fingerprinting: Estimation of Tissue Properties from a Dictionary of Monte Carlo Diffusion MRI Simulations. NeuroImage 184 (January): 964–80.

Roalf, D.R., Quarmley, M., Elliott, M.A., Satterthwaite, T.D., Vandekar, S.N., Ruparel, K., Gennatas, E.D., Calkins, M.E., Moore, T.M., Hopson, R., Prabhakaran, K., Jackson, C.T., Verma, R., Hakonarson, H., Gur R.C., Gur, R.E., 2016. The Impact of Quality Assurance Assessment on Diffusion Tensor Imaging Outcomes in a Large-Scale Population-Based Cohort. NeuroImage 125, 903–19.

Satterthwaite, T.D., Wolf, D.H., Loughead, J., Ruparel, K., Elliott, M.A., Hakonarson, H., Gur, R.C., Gur, R.E., 2012. Impact of in-Scanner Head Motion on Multiple Measures of Functional Connectivity: Relevance for Studies of Neurodevelopment in Youth. NeuroImage 60 (1), 623–32.

Satterthwaite, T.D., Wolf, D.H., Ruparel, K., Erus, G., Elliott, M.A., Eickhoff, S.B., Gennatas, E.D., Jackson, C., Prabhakaran, K., Smith, A., Hakonarson, H., Verma, R., Davatzikos, C., Gur, R.E., Gur, R.C., 2013. Heterogeneous Impact of Motion on Fundamental Patterns of Developmental Changes in Functional Connectivity During Youth. NeuroImage 83, 45-57.

Schaefer, A., Margulies, D.S., Lohmann, G., Gorgolewski, K.J., Smallwood, J., Kiebel, S.J., Villringer, A., 2014. Dynamic Network Participation of Functional Connectivity Hubs Assessed by Resting-State fMRI. Frontiers in Human Neuroscience 8.

Schmithorst, V.J., Yuan. W., 2010. White Matter Development During Adolescence as Shown by Diffusion MRI. Brain and Cognition, Adolescent brain development: Current themes and future directions, 72 (1), 16–25.

Sporns, O., Tononi, G., Kötter., R., 2005. The Human Connectome: A Structural Description of the Human Brain. PLOS Computational Biology 1 (4), e42.

Stanisz, G.J., Wright, G.A., Henkelman, R.M., Szafer, A., 1997. An Analytical Model of Restricted Diffusion in Bovine Optic Nerve. Magnetic Resonance in Medicine 37 (1), 103–11.

Stejskal, E.O., Tanner, J.E., 1965. Spin Diffusion Measurements: Spin Echoes in the Presence of a Time-Dependent Field Gradient. The Journal of Chemical Physics 42 (1), 288–92.

Svolos, P., Kousi, E., Kapsalaki, E., Theodorou, K., Fezoulidis, I., Kappas, C., Tsougos, I. 2014. The Role of Diffusion and Perfusion Weighted Imaging in the Differential Diagnosis of Cerebral Tumors: A Review and Future Perspectives. Cancer Imaging 14 (1), 20.

Theys, C., Wouters, J., Ghesquière, P., 2014. Diffusion Tensor Imaging and Resting-State Functional MRI-Scanning in 5- and 6-Year-Old Children: Training Protocol and Motion Assessment. PLOS ONE 9 (4), e94019.

Turner, R., Le Bihan, D., Chesnicks. A.S., 1991. Echo-Planar Imaging of Diffusion and Perfusion. Magnetic Resonance in Medicine 19 (2), 247–53.

Tustison, N.J., Avants, B.B, Cook, P.A., Zheng, Y., Egan, A., Yushkevich, P.A., Gee, J.C., 2010. N4ITK: Improved N3 Bias Correction. IEEE Transactions on Medical Imaging 29 (6), 1310–20.

Tustison, N.J., Cook, P.A., Klein, A., Song, G., Das, S.R., Duda, J.T., Kandel, B.M., van Strien, N., Stone, J.R., Gee, J.C., Avants, B.B., 2014. Large-Scale Evaluation of Ants and Freesurfer Cortical Thickness Measurements. NeuroImage 99, 166–79.

Uddin, L.Q., Supekar, K.S., Ryali, S., Menon, V., 2011. Dynamic Reconfiguration of Structural and Functional Connectivity Across Core Neurocognitive Brain Networks with Development. Journal Of Neuroscience 31 (50), 18578–89.

Veerart, J., Sijbers, J., Sunaert, S., Leemans, A., Jeurissen, B., 2013. Weighted linear least squares estimations of diffusion MRI parameters: Stengths, limitations, and pitfalls. NeuroImage 81, 335-346.

Volz, L. J., Cieslak, M., Grafton, S.T., 2018. A Probabilistic Atlas of Fiber Crossings for Variability Reduction of Anisotropy Measures. Brain Structure and Function 223 (2), 635–51.

Walter, G.G. 1977. Properties of Hermite Series Estimation of Probability Density. The Annals of Statistics 5 (6), 1258–64.

Wood, S.N., 2001. mgcv: GAMs and generalized ridge regression for R. R News **1**, 20–25

Wood, S.N., 2004. Stable and efficient multiple smoothing parameter estimation for generalized additive models. Journal of the American Statistical Association. 99, 673–686.

Wood, S.N., 2011. Fast stable restricted maximum likelihood and marginal likelihood estimation of semiparametric generalized linear models. Journal of the Royal Statistical Society (B) 73(1):3–36

Yeh, F.C., Verstynen, T.D., Wang, Y., Fernández-Miranda, J.C., Wen-Yih I.T., 2013. Deterministic Diffusion Fiber Tracking Improved by Quantitative Anisotropy. PLOS ONE 8 (11), e80713.

Yendiki, A., Koldewyn, K., Kakunoori, S., Kanwisher, N., Fischl, B., 2014. Spurious Group Differences Due to Head Motion in a Diffusion MRI Study. NeuroImage 88, 79–90.

Zhang, H., Hubbard, P.L., Parker, G.J.M., Alexander, D.C., 2011. Axon diameter mapping in the presence of orientation dispersion with diffusion MRI. NeuroImage, 56(3), 1301–1315.

Zhang, H., Schneider, T., Wheeler-Kingshott, C.A., Alexander, D.C., 2012. NODDI: Practical in Vivo Neurite Orientation Dispersion and Density Imaging of the Human Brain. NeuroImage 61 (4), 1000–1016.